PHYSICAL REVIEW B **95**, 205117 (2017)

Electronic properties of superconducting FeS

C. Tresca,[1,2] G. Giovannetti,[3] M. Capone,[3] and G. Profeta[1,2]
[1]*Department of Physical and Chemical Sciences, University of L'Aquila, Via Vetoio 10, I-67100 L'Aquila, Italy*
[2]*SPIN-CNR, University of L'Aquila, Via Vetoio 10, I-67100 L'Aquila, Italy*
[3]*International School for Advanced Studies (SISSA) and CNR-IOM-Democritos National Simulation Centre,*
Via Bonomea 265, I-34136, Trieste, Italy

(Received 4 June 2016; revised manuscript received 25 January 2017; published 11 May 2017)

We report first-principles density-functional theory results on the electronic and magnetic properties of the recently discovered superconducting FeS, which reveals important differences with the other members of the iron-chalcogenides (FeSe and FeTe). The band structure of FeS is characterized by two hole bands at the Fermi energy with a fully occupied d_{xy} band at Γ. A stripe-antiferromagnetic phase with a small magnetic moment is the most stable magnetic solution, but different magnetic phases have comparable energies indicating a tight competition. Including local interactions treated within dynamical mean-field theory, we find significant correlation effects with orbital-dependent strength and character, even if all the fingerprints of correlations are slightly weaker than in FeSe. The study of the effect of pressure reveals significant changes in the electronic structure of the material and of the correlation effects. These results point toward further studies on the possible superconducting phase stabilized by pressure effects or two dimensionality, in analogy with pressurized and monolayer FeSe.

DOI: 10.1103/PhysRevB.95.205117

I. INTRODUCTION

In the family of iron-based superconductors (FeSC) (for a review on materials properties see Refs. [1,2]), iron-chalcogenides (FeCh) with the PbO phase are attracting a lot of interest for their anomalous properties. The known members of the group are FeSe and FeTe, which are generally referred as 11-family. In these compounds, the $FeCh_4$ tetrahedra planes are the only building blocks of the tetragonal crystal, bound together by the van der Waals interaction [3]. Recently, the chalcogenide family is attracting even more interest because FeSe features a peculiar and appealing phase diagram, and its critical temperature can be boosted up to 100 K when monolayer FeSe is grown on $SrTiO_3$ [4].

Among the members of the FeCh family, FeSe is a superconductor without external doping and/or pressure, with a $T_c = 8$ K [5] and it is characterized by the absence of magnetism and the observation of nematic ordering breaking the lattice rotational symmetry on the plane. Partial substitution of Se with sulfur was found to enhance T_c [6]. On the other hand, FeTe does not present a superconducting phase, but the partial substitution of Te atoms with Se [7] or S [8] induces superconductivity with an optimal concentration around 50% (in $FeTe_{1-x}Se_x$). Tetragonal FeS represents a missing member of the family. FeS crystallizes in the hexagonal phase (pyrrhotite) and is metastable in the tetragonal one (mackinawite). Indeed, the first attempts to observe superconductivity in FeS failed due to the difficulties in stabilizing the tetragonal phase by solid state reactors [9].

The origin of superconducting pairing in FeSC is commonly attributed to the exchange of spin fluctuations with a wave vector $Q = (\pi,\pi)$ [associated with a collinear antiferromagnetic stripe phase (AFM1) [10,11]], which are strongly influenced by the structural degree of freedom. In fact, superconductivity in FeSe can be boosted by pressure (it can reach 37 K applying a pressure of about 9 GPa [12]) and suppressed by tensile strain [13].

The coupling among structural, magnetic, and superconducting phases is evident observing that also electronic correlation effects increase with the chalcogen height from the iron plane: in FeTe, Te atom is at 1.75 Å above the Fe plane resulting in a strongly correlated phase detected by ARPES [14], transport [15], optical measurements [16], and STM/STS experiments [17]; FeSe results in an intermediate situation, with Se height of 1.46 Å, in which, spin fluctuations do not stabilize any magnetic structures.

Furthermore, dynamical mean-field theory (DMFT) and related methods have highlighted the role of the Hund's coupling in driving a strongly correlated metallic state in different compounds in the iron-based family [18–22] including FeCh [19,20] despite that most materials of the family appear far from the Mott localization. The degree of correlation is strongly dependent on the orbital (or orbital-selective) [23–28] as a result of an effective orbital decoupling driven by the Hund's interaction [21,29].

Thus the stabilization of the tetragonal phase (PbO type) of FeS and the study of its superconducting state would complete the characterization of the FeCh family, providing us with important information about the role of structural properties, magnetism, correlations, and nematic behavior for the stabilization of the superconducting phase within this family of materials.

An important step in this direction has been made by Lai *et al.* [30] who, using the hydrothermal method of iron powder with sulfide solution, reported the successful growth of stoichiometric FeS and observed a superconducting transition at $T_c \sim 5$ K, a value of the same order as in FeSe at ambient pressure.

At the moment, the available experimental information on FeS evidences the absence of magnetic order [31,32] or small magnetic moment on the iron site [33]. Scanning tunnel microscopy/spectroscopy (STM/STS) experiments [34] reveal a slight difference in the lattice constants reminiscent of FeSe nematic phase and suggest relatively strong-coupling superconductivity. Specific heat measurements suggest the presence of one (or two) nodal gap(s) [35] and recent STM/STS experiments [34] are compatible, within the Dynes model fit [36], with an anisotropic s-wave or $(s + d)$-wave symmetry of the gap. The system shows the largest anisotropy of all FeSC, as measured by the ratio of the upper critical fields in two orthogonal directions [37]. Very recently, high-pressure experiments have shown a rapid decrease of superconductivity by increasing pressure followed, for even larger pressures, by a second superconducting state with a maximum T_c of 6 K at 15 GPa [38]. On the other hand, early density-functional theory (DFT) simulations reported conflicting results where both magnetic [39] and nonmagnetic [40] solutions are obtained.

The purpose of this work is to study, by first-principles DFT and DMFT, the structural, electronic, magnetic, and correlation properties of FeS, and to put on a firmer ground the understanding of the microscopic effects at work in the development of the superconducting phase, trying to compare its properties with other chalcogenides, FeSe, in particular.

II. COMPUTATIONAL DETAILS

Theoretical calculations were performed using the Vienna *ab initio* simulation package (VASP) [41,42], using the generalized gradient approximation (GGA) [43] for the exchange-correlation energy. Since in FeCh systems the out-of-plane van der Waals (vdW) interaction cannot be neglected [3], we will include it as a dispersive term, using the DFT-D2 Grimme's semiempirical correction [44], along the c direction.

We used projected augmented-wave (PAW) pseudopotentials [45] for all the atomic species involved, with an energy cutoff up to 350 eV. Integration over the Brillouin zone (BZ) was performed using uniform Monkhorst and Pack grid [46] of 16 × 16 × 10 for sampling BZ using a Gaussian smearing with $\sigma = 0.02$ eV.

To understand the role of electron-electron interactions, we consider the DFT+DMFT [47] method, which treats exactly the local quantum dynamics mapping the lattice model onto an impurity embedded in a self-consistent bath. On the other hand, nonlocal correlations are treated as in a static mean-field approach. The method becomes indeed exact when the self-energy does not depend on momentum, but it allows for an arbitrarily rich frequency dependence. Within this approach, we include the on-site interactions (Hubbard U and Hund's coupling) starting from localized orbitals, which we define as maximally localized Wannier orbitals [48] for the pure $3d$ Fe orbitals built from the iron bands in the energy range between −3 and 2.5 eV.

For the interacting part of the Hamiltonian, we use the Kanamori type

$$\begin{aligned}H_{\text{int}} = {} & U\sum_{i,m} n_{im\sigma}n_{im\sigma'} + U'\sum_{i,m,m'} n_{im\sigma}n_{im'\sigma'} \\ & + U^{''}\sum_{i,m,m'} n_{im\sigma}n_{im'\sigma} \\ & - J_h\sum_{i,m,m'}[d^{+}_{im\uparrow}d^{+}_{im'\downarrow}d_{im\downarrow}d_{im'\uparrow} + d^{+}_{im\uparrow}d^{+}_{im\downarrow}d_{im'\uparrow}d_{im'\downarrow}],\end{aligned}$$

where $d_{i,m\sigma}$ is the destruction operator of an electron of spin σ at site i in orbital m, and $n_{im\sigma} = d^{+}_{im\sigma}d_{im\sigma}$, U and $U' = U - 2J_h$, $U^{''} = U - 3J_h$ are intra- and interorbital repulsions and J_h is the Hund's coupling.

In the absence of *ab initio* values of U and J_h for this material, we used the constrained random-phase approximation estimates for FeSe ($U = 4.2$ eV and $J_h = 0.504$ eV) computed in Ref. [49]. In the same paper, the authors show that the Hubbard U increases from FeTe to FeSe [49] and thus we expect an even larger value for FeS. However, it has been suggested that the degree of correlation depends only weakly on U in the realistic physical range [20,21,24]. On the other hand, the correlations are more sensitive on the value of J_h, which, however, varies much less from FeTe to FeSe.

To solve the impurity model at zero temperature, we use exact diagonalization [50,51]. We consider $N_s = 15$ orbitals in total, with five impurity orbitals and two bath degrees of freedom connected to each impurity orbital. The Hamiltonian conserves the number of particles and the sectors with different number of particles are independently diagonalized, which leads to a largest Hilbert space of dimension 41 409 225. The massive storage requirements are met exploiting a parallel Arnoldi algorithm and implementing spin-inversion symmetry [52].

III. STRUCTURAL, ELECTRONIC, AND MAGNETIC PHASES

As demonstrated for other iron-based superconductors, DFT predictions of the structural properties strongly depend on the considered electronic state. In particular, it has been shown that the best agreement with experiments is generally obtained in magnetic calculations, which partially include the effect of spin fluctuations [15]. We, thus, performed structural optimization of the lattice parameters considering several competitive phases: nonmagnetic phase (NM), checkerboard (AFM0), stripe-antiferromagnetic (AFM1), bicollinear (AFM2), and double-checkerboard (plaquette) (AFM3) [53].

First of all, considering the experimental lattice constants (from Ref. [30]), we predict the AFM1 stripe phase as the ground state. Relaxation of the internal parameter z_S (height of S atom above the iron plane) does not change the conclusion. AFM0 and AFM2 phases can not be stabilized in FeS, while the energy of the AFM3 one is about 1 meV per atom higher than that of AFM1 (at the experimental structural parameters). In analogy with FeSe, the two magnetic phases are close in energy explaining, in part, the lack of experimental confirmation of the magnetic phase [54,55].

The structural parameters obtained minimizing the total energy in the magnetic stripe-phase are summarized in Table I. Results with and without the inclusion of van der Waals interaction are also shown. The inclusion of this additional energy term was already demonstrated to be essential for the proper description of the structural parameters in FeSe and FeTe [3]. Even if the agreement between theoretical and experimental lattice constants is within the degree of accuracy of DFT, considering the computational complexity and peculiarities of iron-based superconductors [56], the 4%– 5% error in the out-of-plane lattice parameter can highlight peculiar features not captured by mean-field DFT. A comparison with the other

TABLE I. Calculated lattice parameters of FeS in the AFM1 phase (see text) with and without vdW contribution (the *a* lattice vector points along the FM direction, *b* along the AFM one).

	GGA	GGA+vdW	Exp. [30]
a (Å)	3.58(0)	3.54(5)	3.68(0)
b (Å)	3.58(1)	3.55(2)	3.68(0)
c (Å)	5.29	4.79	5.03(0)
h_S (Å)	1.21	1.22	1.27
$\mu_{\mathrm{Fe}}(\mu_B)$	0.034	0.320	—

FeCh shows a clear decreasing trend in the height of the chalcogen atoms Te, Se and S in iron-chalcogenides materials.

The small value of this distance leads to a very small magnetic moment that we estimate as 0.32 μ_B, much smaller than the values obtained for FeSe (1.96 μ_B) and FeTe (2.37 μ_B), and it drops to an essentially zero value if we neglect the van der Waals interaction between consecutive FeS planes. As a consequence, the magnetostriction effect, which leads to a reduction of in-plane lattice constant along the FM direction and an expansion on the AFM one, is negligible (differences of the order of 0.3%) due to the small magnetic moment on the Fe sites.

The sensitivity of the magnetic moment to the chalcogen height is demonstrated in Fig. 1, in which we report the total energy of the system and the magnetic moment on Fe ions as a function of z_S internal parameter, fixing the lattice constants at the experimental values. It is worth to mention that, using the experimental lattice constant and internal parameters, the calculated magnetic moment sensibly increases to 1.52 μ_B. The magnetic moment increases with z_S as in other Fe-based superconducting materials [57], vanishing at a critical height $h_S = 1.11$ Å ($z_S = 0.22$). This points to possible stabilization of high magnetic moment phases, induced by in-plane compressive strain (growth on suitable substrates) [53] or nonhydrostatic pressure effects [58].

A. Electronic structure

In Fig. 2, we report the band structure along the high-symmetry directions of the irreducible BZ of the tetragonal lattice for the nonmagnetic and AFM1 phases using the experimental structural parameters. The low-energy manifold of FeS has a bandwidth of 5.3 eV, essentially identical to FeSe and the overall band structure resembles that of the other FeCh, but with important differences. In particular, in the nonmagnetic band structure, there are two hole bands crossing the Fermi level around the Γ point and two electron bands around the *M* point forming two-dimensional cylinders. The two dimensionality of the electronic bands is confirmed by the negligible dispersion along the Γ-*Z* line. On the other hand, we recall that in both FeSe and FeTe, DFT predicts three holelike cylinders around the Γ point. In FeS, the d_{xy} band is completely filled at Γ due to the smaller h_S height. The same result is, for example, obtained with FeSe under strain [53]. The magnetic phase shows a reduction of the density of states at the Fermi energy, characterized by an insulating-like band structure in the Γ-*X*-*M* plane of the BZ. However, the system is metallic with only one band crossing the Fermi energy in the *Z*-*R*-*A* plane.

It is nowadays well established that electron-electron interactions play a relevant role in all the materials in the iron-based family, even if there is no agreement on their relevance for superconductivity, magnetism, and nematicity. In particular, it has been shown that the sizable value of the Hund's coupling plays a major role [18] leading to a variety of phenomena including a strongly correlated metallic regime [18] far from a Mott transition [59], a dichotomy between instantaneous

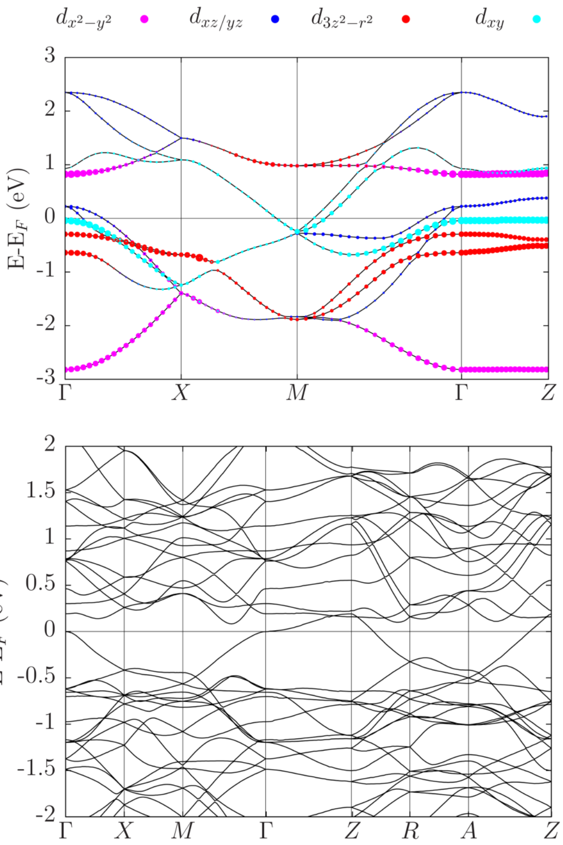

FIG. 2. Band structure of FeS along the high-symmetry direction of Brillouin zone for nonmagnetic (upper panel) and AFM1 phase (lower panel). The main orbital character of the Kohn-Sham states is highlighted with different colors.

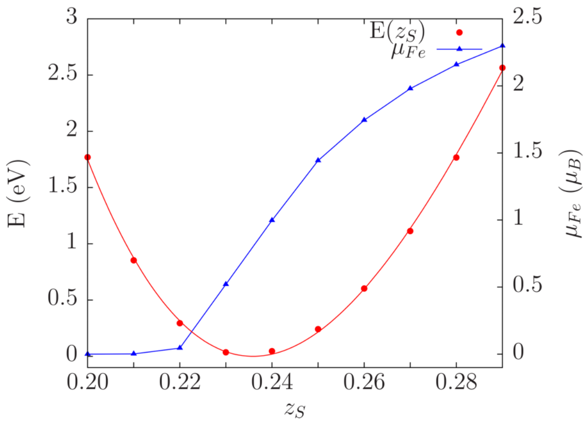

FIG. 1. Total energy (magnetic moment on the iron site) as a function of z_S on left (right) *y* axis. Lines are a guide for eyes.

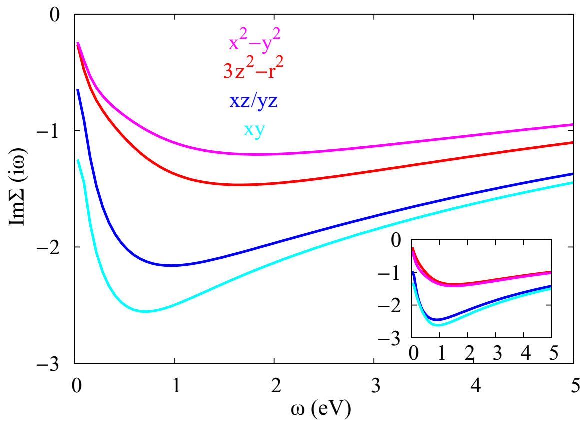

FIG. 3. Orbital-resolved imaginary part of local self-energy [$\Sigma(i\omega)$] as a function of the Matsubara imaginary frequency within DFT + DMFT for FeS and FeSe (inset) using the same interaction strengths $U = 4.2$ eV and $J_h = 0.504$ eV.

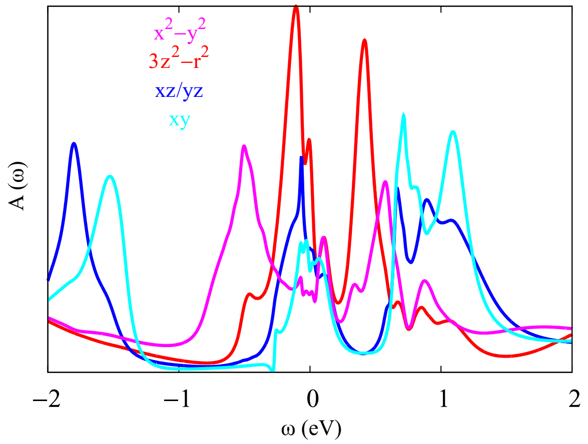

FIG. 4. Orbital-resolved spectral function $A(\omega)$ as a function of real frequency within DFT + DMFT for FeS with $U = 4.2$ eV and $J_h = 0.504$ eV.

and long-time spin correlations [21], a strong dependence of correlation effects on the orbital degree of freedom [21], anomalous power-law behavior of spectral properties [60], and an enhancement of the charge compressibility, which in turn may favor other instabilities [61]. In the case of FeSe, Hund-driven correlations have also been connected with the observed nematic instability [62]. DMFT has been largely used to study FeSC and it helped our understanding of the anomalies of the metallic states.

For this reason, we complement the DFT analysis with a DMFT treatment of the local correlations as discussed above. In Fig. 3, we report the orbital-resolved imaginary part of the self-energy on the imaginary-frequency axis, which we compare for reference with analogous calculations for FeSe. The choice of using the same value of the interaction highlights the role of the different band structure.

The self-energy measures the effect of the interactions on the single-particle properties. The results for FeS suggest rather important correlation effects as measured by the overall values of the self-energies, which are comparable with the results for FeSe [63] and a rather pronounced dependence on the orbital, with a larger degree of correlation for t_{2g} orbitals and in particular for the xy. At low frequency, the imaginary part of the self-energies appear to extrapolate to a finite value, which would imply a non-Fermi liquid incoherent metallic state with a finite lifetime for the low-energy excitations. For this reason, we can not provide values for the quasiparticle weight Z, which is not defined for a non-Fermi liquid. Overall, the results are qualitatively similar to those for FeSe [19], which we report in the inset of Fig. 3 using exactly the same solver we employ for FeS. A closer comparison shows that all the effects we highlighted (size of the self-energies, orbital differentiation, breakdown of the Fermi liquid) are slightly more pronounced in FeSe.

The orbital differentiation is common to the other chalcogenides [20,21] and it has been ascribed to the orbital decoupling effect of the Hund's coupling. In particular, in Ref. [21], it has been shown that in the 122 family the degree of correlation of each orbital is essentially controlled by its distance from half-filling. Therefore the orbitals with an occupation per spin close to 0.5 should be more correlated than the others. Indeed, the DFT+DMFT occupations per spin of the $3z^2 - r^2$, xz, yz, $x^2 - y^2$, xy orbitals are respectively (0.69, 0.55, 0.55, 0.70, 0.51), which perfectly fits in the above classification confirming the generality of this result.

In Fig. 4, we show the orbital-resolved spectral density in DFT+DMFT (obtained by the Padé approximation starting from the imaginary-frequency Green's functions) in which the effects of electronic correlations on the single-particle spectra clearly emerge. The relatively broad DFT bands substantially shrink due to electron-electron interactions, confining the quasiparticle excitations in a region of 1 eV around the Fermi level, while predominant spectral weight with character of t_{2g} orbitals is shifted to high energy as observed in FeSe [19]. This result is reiterated by the momentum-resolved spectral function plotted in Fig. 5, which confirms the strong renormalization of the electron bandwidth of the 3d orbitals with respect to the DFT results, which we estimate to be of about a factor of 3.

All our results can be summarized in the observation that correlation effects in FeS share many similarities with those of FeSe and are simply slightly weaker. This reduction of

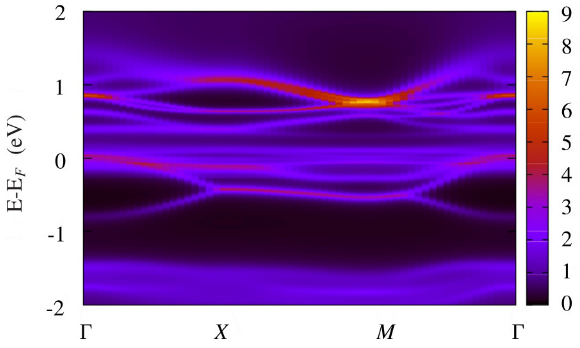

FIG. 5. DFT + DMFT band structure of FeS calculated at $U = 4.2$ eV and $J_h = 0.504$ eV.

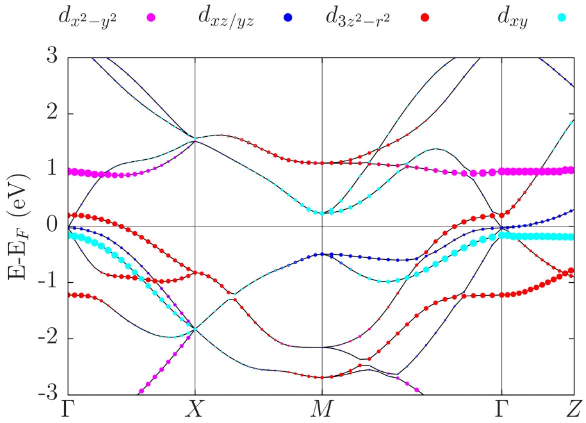

FIG. 6. Band structure of FeS at 15 GPa along the high-symmetry directions of Brillouin zone for nonmagnetic phase. The main orbital character of the Kohn-Sham states are highlighted with different colors.

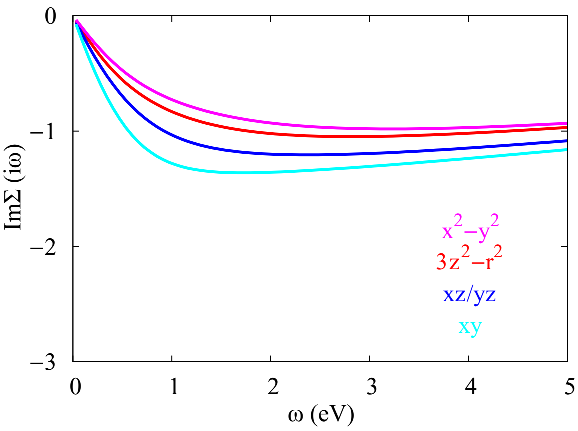

FIG. 7. Orbital-resolved imaginary part of local self-energy (Σ) as a function of the Matsubara imaginary frequency within DFT + DMFT for FeS at 15 GPa.

correlations can be directly connected with the compression of lattice parameters and height of the chalcogen ion.

The similarity of the low-energy properties with FeSe and the observed increase of it superconducting critical temperature in the high-pressure phase, call for a study of FeS in the high pressure region. High-pressure experiments [38] reported a structural phase transition of FeS starting from 7.2 GPa, from the tetragonal phase at ambient pressure to the hexagonal (semiconducting) phase. The optimal T_c is achieved around 15 GPa and attributed to residual high pressure (metastable) tetragonal phase.

We predicted the lattice parameters at 15 GPa finding a slight reduction of the a parameter ($a = 3.52$ Å at 15 GPa), while the out-of-plane c lattice constants is sensibly reduced ($c = 4.08$ Å at 15 GPa). This determines a complete disappearance of magnetism and interesting changes in the band structure, which are reported in Fig. 6.

The main effect of pressure is to promote a topological transition at the high symmetry points (Γ and M) with respect to the band structure at ambient pressure (Fig. 2). In particular, at the Γ point, the d_{xy} is completely occupied, while the $d_{3z^2-r^2}$ band (occupied at ambient pressure) is pushed above the Fermi level, giving rise to a new Fermi surface sheet. Interestingly, the antibonding $d_{xz/yz}$ exchange degeneracy and give rise to the linear dispersing bands near the Γ point, touching at the Fermi energy. A similar behavior was already highlighted in FeSe$_x$Te$_{1-x}$, which has nontrivial Z_2 topological invariance, which originates from the parity exchange at the Γ point of BZ as a function of the lattice parameters [64]. In the case of FeS, the enhanced three dimensionality has even more dramatic consequences: the complete disappearance of electronic Fermi surface at the M point, being thus characterized by a single Fermi surface with $d_{3z^2-r^2}$ character and two 3D Fermi surfaces around A point with d_{xy} character.

The topological change of the Fermi surface as a function of the pressure and strain is a common effect in iron-based superconductors, which is often linked with dramatic discontinuities of the superconducting critical temperature: CaFe$_2$As$_2$ under pressure [65], KFe$_2$As$_2$ [66–68], monolayer FeSe on SrTiO$_3$ [53,69]. Therefore, if confirmed, the observation of superconductivity in single-band FeS under pressure poses important questions on the origin of the superconducting phase and the symmetry of the superconducting order parameter. As proposed to explain the so-called V-shape behavior of the critical temperature as a function of pressure, $T_c(P)$, in KFe$_2$As$_2$ [70], one might expect a change of symmetry also for FeS, where the low pressure superconducting phase with a likely $s^{\pm}$ order parameter can be replaced by a possible d-wave the high pressure phase.

The bandwidth of the FeS under pressure is increased up to 11 eV, significantly larger than the ambient-pressure value. As a consequence, the degree of correlation is expected to be substantially reduced. Our DMFT calculations for FeS under pressure confirm this expectation, showing imaginary parts of the self-energies, which are reduced by more than a factor of two and smoothly extrapolate to zero at small frequency as expected in a normal Fermi liquid (see Fig. 7). In this case, we can evaluate the quasiparticle weight Z obtaining the following orbital resolved values: $Z_{3z^2-r^2} = 0.448$, $Z_{xz/yz} = 0.363$, $Z_{x^2-y^2} = 0.484$, and $Z_{xy} = 0.318$. This makes FeS under pressure a much more conventional metal with only quantitative corrections due to the electron-electron interactions.

IV. CONCLUSIONS

We have studied the interplay between structural and electronic properties, magnetism and strong correlation in FeS both in ambient conditions and at large pressure, where a second superconducting dome is experimentally observed. The qualitative features of the normal state properties and the correlation strengths in FeS are similar to what is observed in FeSe, pointing towards a similar description of its physical properties. However, important differences can give rise to new and unanticipated phenomena: (i) presence of two hole Fermi surfaces around the Γ point, (ii) lattice parameters sensibly different with respect to FeSe, making FeS a "compressed" version of FeSe, (iii) reduced magnetic moment and structural distortions with respect to FeSe, and (iv) topological transitions under high pressure, not observed in FeSe, resulting in a single Fermi surface in the Γ-X-M plane at 15 GPa.

The discovery of superconductivity in pure FeS is important for many reasons, which goes well beyond the value of its critical temperature, representing a missing piece in the puzzle of iron-chalcogenide family. We believe that further experimental studies and characterizations of FeS can disentangle important aspects to understand the complex phenomenology of iron-chalcogenide superconductors.

Note added. During the editorial review process of the present paper, two studies appeared reporting experimental results of FeS [71,72], which confirms many of the conclusions of the present paper. In the first one, the authors found that FeS is a tetragonal paramagnet with reduced quasiparticle mass from that of FeSe, concluding that FeS is less correlated than FeSe, as we predict by DMFT. In addition, neutron scattering finds only stripe-type spin excitations up to 100 meV, in agreement with our first-principles ground-state magnetic phase. In the second paper [72], the first ARPES spectra of FeS appeared in the literature. The authors find only two holelike Fermi surfaces, instead of the expected three as in other iron-based superconductors, attributing this discrepancy to defect scattering. However, based on our results, this experimental evidence confirms our theoretical prediction. On the other hand, the number of electronlike Fermi surface found in the experiment is two, even in this case in perfect agreement with our calculations. Also, the measured bandwidth renormalization with respect to mean-field DFT bands, estimated to be within 3 and 2.5 [72], agree with our estimation of 3.

ACKNOWLEDGMENTS

The research leading to these results received financial support by from the European Union under FP7 ERC Starting Grant No. 240524 “SUPERBAD” and the joint SISSA-CNR project Prot. SISSA N.232/2015. We thank L. de’ Medici and L. Fanfarillo for helpful discussions and acknowledge the Supercomputing center Cineca (Bologna, Italy) for computational support through ISCRA projects. M.C. acknowledges support of MIUR through the PRIN 2015 program (Prot. 2015C5SEJJ001).

[1] G. R. Stewart, Rev. Mod. Phys. **83**, 1589 (2011).

[2] H. Hosono and K. Kuroki, Physica C **514**, 399 (2015).

[3] F. Ricci and G. Profeta, Phys. Rev. B **87**, 184105 (2013).

[4] J.-F. Ge, Z.-L. Liu, C. Liu, C.-L. Gao, D. Qian, Q.-K. Xue, Y. Liu, and J.-F. Jia, Nat. Mater. **14**, 285 (2015).

[5] F.-C. H. *et al.*, Proc. Natl. Acad. Sci. USA **105**, 14262 (2008).

[6] Y. Mizuguchi, F. Tomioka, S. Tsuda, T. Yamaguchi, and Y. Takano, J. Phys. Soc. Jpn. **78**, 074712 (2009).

[7] K.-W. Yeh, T.-W. Huang, Y. lin Huang, T.-K. Chen, F.-C. Hsu, P. M. Wu, Y.-C. Lee, Y.-Y. Chu, C.-L. Chen, J.-Y. Luo, D.-C. Yan, and M.-K. Wu, EPL **84**, 37002 (2008).

[8] Y. Mizuguchi, F. Tomioka, S. Tsuda, T. Yamaguchi, and Y. Takano, Appl. Phys. Lett. **94**, 012503 (2009).

[9] L. A. Taylor and L. W. Finger, Carnegie Institute of Washington, Geophys. Lab. Ann. Rept. **69**, 318 (1970).

[10] J. Paglione and R. L. Greene, Nat. Phys. **6**, 645 (2010).

[11] F. Wang and D.-H. Lee, Science **332**, 200 (2011).

[12] S. Medvedev *et al.*, Nat. Mater. **8**, 630 (2009).

[13] Y. F. Nie, E. Brahimi, J. I. Budnick, W. A. Hines, M. Jain, and B. O. Wells, Appl. Phys. Lett. **94**, 242505 (2009).

[14] A. Tamai, A. Y. Ganin, E. Rozbicki, J. Bacsa, W. Meevasana, P. D. C. King, M. Caffio, R. Schaub, S. Margadonna, K. Prassides, M. J. Rosseinsky, and F. Baumberger, Phys. Rev. Lett. **104**, 097002 (2010).

[15] F. Caglieris, F. Ricci, G. Lamura, A. Martinelli, A. Palenzona, I. Pallecchi, A. Sala, G. Profeta, and M. Putti, Sci. Technol. Adv. Mater. **13**, 054402 (2012).

[16] G. F. Chen, Z. G. Chen, J. Dong, W. Z. Hu, G. Li, X. D. Zhang, P. Zheng, J. L. Luo, and N. L. Wang, Phys. Rev. B **79**, 140509 (2009).

[17] A. Gerbi, R. Buzio, S. Kawale, E. Bellingeri, A. Martinelli, C. Bernini, C. Tresca, M. Capone, G. Profeta, and C. Ferdeghini (unpublished).

[18] K. Haule and G. Kotliar, New J. Phys. **11**, 025021 (2009).

[19] M. Aichhorn, S. Biermann, T. Miyake, A. Georges, and M. Imada, Phys. Rev. B **82**, 064504 (2010).

[20] N. Lanatà, H. U. R. Strand, G. Giovannetti, B. Hellsing, L. de’ Medici, and M. Capone, Phys. Rev. B **87**, 045122 (2013).

[21] L. de’ Medici, G. Giovannetti, and M. Capone, Phys. Rev. Lett. **112**, 177001 (2014).

[22] R. Yu and Q. Si, Phys. Rev. B **84**, 235115 (2011).

[23] L. de’ Medici, S. R. Hassan, M. Capone, and X. Dai, Phys. Rev. Lett. **102**, 126401 (2009).

[24] Z. P. Yin, K. Haule, and G. Kotliar, Nat. Phys. **7**, 294 (2011).

[25] Z. P. Yin, K. Haule, and G. Kotliar, Nat. Mater. **10**, 932 (2011).

[26] Z. Wang, V. Tsurkan, M. Schmidt, A. Loidl, and J. Deisenhofer, Phys. Rev. B **93**, 104522 (2016).

[27] Y. Liu, D.-Y. Liu, J.-L. Wang, J. Sun, Y. Song, and L.-J. Zou, Phys. Rev. B **92**, 155146 (2015).

[28] M. Yi, Z.-K. Liu, Y. Zhang, R. Yu, J. X. Zhu, J. J. Lee, R. G. Moore, F. T. Schmitt, W. Li, S. C. Riggs, J. H. Chu, B. Lv, J. Hu, M. Hashimoto, S. K. Mo, Z. Hussain, Z. Q. Mao, C. W. Chu, I. R. Fisher, Q. Si, Z. X. Shen, and D. H. Lu, Nat. Commun. **6**, 7777 (2015).

[29] L. Fanfarillo and E. Bascones, Phys. Rev. B **92**, 075136 (2015).

[30] X. Lai, H. Zhang, Y. Wang, X. Wang, X. Zhang, J. Lin, and F. Huang, J. Am. Chem. Soc. **137**, 10148 (2015).

[31] E. Bertaut, P. Burlet, and J. Chappert, Solid State Commun. **3**, 335 (1965).

[32] D. Vaughan and M. Ridout, J. Inorgan. Nuclear Chem. **33**, 741 (1971).

[33] S. Holenstein, U. Pachmayr, Z. Guguchia, S. Kamusella, R. Khasanov, A. Amato, C. Baines, H.-H. Klauss, E. Morenzoni, D. Johrendt, and H. Luetkens, Phys. Rev. B **93**, 140506 (2016).

[34] X. Yang, Z. Du, G. Du, Q. Gu, H. Lin, D. Fang, H. Yang, X. Zhu, and H.-H. Wen, Phys. Rev. B **94**, 024521 (2016).

[35] J. Xing, H. Lin, Y. Li, S. Li, X. Zhu, H. Yang, and H.-H. Wen, Phys. Rev. B **93**, 104520 (2016).

[36] R. C. Dynes, V. Narayanamurti, and J. P. Garno, Phys. Rev. Lett. **41**, 1509 (1978).

[37] C. K. H. Borg, X. Zhou, C. Eckberg, D. J. Campbell, S. R. Saha, J. Paglione, and E. E. Rodriguez, Phys. Rev. B **93**, 094522 (2016).

[38] J. Zhang, F. L. Liu, T. P. Ying, N. N. Li, Y. Xu, L. P. He, X. C. Hong, Y. J. Yu, M. X. Wang, W. G. Yang, and S. Y. Li, arXiv:1604.05254.

[39] J. Brgoch and G. J. Miller, J. Phys. Chem. A **116**, 2234 (2012).

[40] A. Subedi, L. Zhang, D. J. Singh, and M. H. Du, Phys. Rev. B **78**, 134514 (2008).

[41] G. Kresse and J. Furthmüller, Phys. Rev. B **54**, 11169 (1996).

[42] G. Kresse and J. Furthmüller, Comp. Mater. Sci. **6**, 15 (1996).

[43] G. Kresse and D. Joubert, Phys. Rev. B **59**, 1758 (1999).

[44] S. Grimme, J. Comp. Chem. **27**, 1787 (2006).

[45] P. E. Blöchl, Phys. Rev. B **50**, 17953 (1994).

[46] H. J. Monkhorst and J. D. Pack, Phys. Rev. B **13**, 5188 (1976).

[47] A. Georges, G. Kotliar, W. Krauth, and M. J. Rozenberg, Rev. Mod. Phys. **68**, 13 (1996).

[48] A. A. Mostofi, J. R. Yates, Y.-S. Lee, I. Souza, D. Vanderbilt, and N. Marzari, Comp. Phys. Commun. **178**, 685 (2008).

[49] T. Miyake, K. Nakamura, R. Arita, and M. Imada, J. Phys. Soc. Jpn. **79**, 044705 (2010).

[50] M. Caffarel and W. Krauth, Phys. Rev. Lett. **72**, 1545 (1994).

[51] M. Capone, L. de' Medici, and A. Georges, Phys. Rev. B **76**, 245116 (2007).

[52] G. Giovannetti, L. de' Medici, M. Aichhorn, and M. Capone, Phys. Rev. B **91**, 085124 (2015).

[53] C. Tresca, F. Ricci, and G. Profeta, 2D Mater. **2**, 015001 (2015).

[54] A. E. Böhmer, T. Arai, F. Hardy, T. Hattori, T. Iye, T. Wolf, H. v. Löhneysen, K. Ishida, and C. Meingast, Phys. Rev. Lett. **114**, 027001 (2015).

[55] Q. Wang, Y. Shen, B. Pan, Y. Hao, M. Ma, F. Zhou, P. Steffens, K. Schmalzl, T. R. Forrest, M. Abdel-Hafiez, X. Chen, D. A. Chareev, A. N. Vasiliev, P. Bourges, Y. Sidis, H. Cao, and J. Zhao, Nat. Mater. **15**, 159 (2016).

[56] P. J. Hirschfeld, M. M. Korshunov, and I. I. Mazin, Rep. Prog. Phys. **74**, 124508 (2011).

[57] G. Giovannetti, C. Ortix, M. Marsman, M. Capone, J. van den Brink, and J. Lorenzana, Nat. Commun. **2**, 398 (2011).

[58] N. Colonna, G. Profeta, and A. Continenza, Phys. Rev. B **83**, 224526 (2011).

[59] L. de' Medici, J. Mravlje, and A. Georges, Phys. Rev. Lett. **107**, 256401 (2011).

[60] Z. P. Yin, K. Haule, and G. Kotliar, Phys. Rev. B **86**, 195141 (2012).

[61] L. de' Medici, Phys. Rev. Lett. **118**, 167003 (2017).

[62] L. Fanfarillo, G. Giovannetti, M. Capone, and E. Bascones, Phys. Rev. B **95**, 144511 (2017).

[63] A. Liebsch and H. Ishida, Phys. Rev. B **82**, 155106 (2010).

[64] Z. Wang, P. Zhang, G. Xu, L. K. Zeng, H. Miao, X. Xu, T. Qian, H. Weng, P. Richard, A. V. Fedorov, H. Ding, X. Dai, and Z. Fang, Phys. Rev. B **92**, 115119 (2015).

[65] R. S. Gonnelli, D. Daghero, M. Tortello, G. A. Ummarino, Z. Bukowski, J. Karpinski, P. G. Reuvekamp, R. K. Kremer, G. Profeta, K. Suzuki, and K. Kuroki, Sci. Rep. **6**, 26394 (2016).

[66] Y. Nakajima, R. Wang, T. Metz, X. Wang, L. Wang, H. Cynn, S. T. Weir, J. R. Jeffries, and J. Paglione, Phys. Rev. B **91**, 060508 (2015).

[67] D. Guterding, S. Backes, H. O. Jeschke, and R. Valentí, Phys. Rev. B **91**, 140503 (2015).

[68] C. Tresca and G. Profeta, Phys. Rev. B **95**, 165129 (2017).

[69] S. Tan, Y. Zhang, M. Xia, Z. Ye, F. Chen, X. Xie, R. Peng, D. Xu, Q. Fan, H. Xu, J. Jiang, T. Zhang, X. Lai, T. Xiang, J. Hu, B. Xie, and D. Feng, Nat. Mater. **12**, 634 (2013).

[70] F. F. Tafti, A. Ouellet, A. Juneau-Fecteau, S. Faucher, M. Lapointe-Major, N. Doiron-Leyraud, A. F. Wang, X.-G. Luo, X. H. Chen, and L. Taillefer, Phys. Rev. B **91**, 054511 (2015).

[71] H. Man, J. Guo, R. Zhang, R. Schönemann, Z. Yin, M. Fu, M. B. Stone, Q. Huang, Y. Song, W. Wang, D. J. Singh, F. Lochner, T. Hickel, I. Eremin, L. Harriger, J. W. Lynn, C. Broholm, L. Balicas, Q. Si, and P. Dai, Quantum Mater. **2**, 14 (2017).

[72] J. Miao, X. H. Niu, D. F. Xu, Q. Yao, Q. Y. Chen, T. P. Ying, S. Y. Li, Y. F. Fang, J. C. Zhang, S. Ideta, K. Tanaka, B. P. Xie, D. L. Feng, and F. Chen, arXiv:1703.08682.